



**HAL**  
open science

## Direction-Dependent Elastic Grain-Interaction Models

Udo Welzel, Sylvain Fréour, Eric J. Mittemeijer

► **To cite this version:**

Udo Welzel, Sylvain Fréour, Eric J. Mittemeijer. Direction-Dependent Elastic Grain-Interaction Models: A Comparative Study. *Philosophical Magazine*, 2005, 85, pp.2391-2414. 10.1080/14786430500070685 . hal-01006751

**HAL Id: hal-01006751**

**<https://hal.science/hal-01006751>**

Submitted on 3 Feb 2018

**HAL** is a multi-disciplinary open access archive for the deposit and dissemination of scientific research documents, whether they are published or not. The documents may come from teaching and research institutions in France or abroad, or from public or private research centers.

L'archive ouverte pluridisciplinaire **HAL**, est destinée au dépôt et à la diffusion de documents scientifiques de niveau recherche, publiés ou non, émanant des établissements d'enseignement et de recherche français ou étrangers, des laboratoires publics ou privés.

# Direction-dependent elastic grain-interaction models – a comparative study

U. WELZEL\*, S. FRÉOUR and E. J. MITTEMEIJER

Max Planck Institute for Metals Research, Heisenbergstrasse 3,  
D-70569 Stuttgart, Germany

Mechanical and diffraction (X-ray) elastic constants (diffraction (X-ray) stress factors for macroscopically elastically anisotropic specimens) can be calculated for polycrystalline specimens from single-crystal elastic data by employing elastic grain-interaction models. Traditionally, only so-called *isotropic* grain-interaction models are considered: all directions in the polycrystal are taken equivalent with respect to the grain interaction. Only recently, so-called direction-dependent, i.e. *anisotropic* grain-interaction models, have been proposed. These models can express the effects of the reduced dimensionality of thin films, of the surface anisotropy of bulk polycrystals and of a grain-shape (morphological) texture on the elastic properties of polycrystals. In this work, the available, recently proposed direction-dependent grain-interaction models will be compared, in particular on the basis of numerical calculations of diffraction and mechanical elastic constants, of variances of certain orientation-dependent stress and strain tensor components and of the distributions of strains in the Euler (orientation) space. It will be demonstrated that the so-called Vook–Witt and inverse Vook–Witt models become (but only approximate) equivalent to the Eshelby–Kröner model for certain grain-shape textures.

## 1. Introduction

Grain-interaction models describe the distribution of stresses and strains over the (crystallographically) differently oriented grains in a polycrystalline specimen subjected to an internal or external load. By adopting a grain-interaction model, macroscopic, mechanical elastic constants, relating mechanical strains to mechanical stresses, and diffraction (X-ray) elastic constants (diffraction (X-ray) stress factors for macroscopically elastically anisotropic samples), relating (diffraction) lattice strains to mechanical stresses, can be calculated for polycrystals from single-crystal elastic data of the individual grains composing the polycrystal [1, 2].

Traditionally, the Reuss [3], Voigt [4], Neerfeld [5]–Hill [6] and the Eshelby [7] Kröner [8, 9] models are employed. These models can be called *isotropic* grain-interaction models [2]: for all directions in the polycrystal, the same grain-interaction

---

\*Corresponding author. Email: u.welzel@mf.mpg.de

assumptions are adopted. It is common to all the above-mentioned, traditional grain-interaction models that they assume that a polycrystal is mechanically elastically isotropic in the absence of crystallographic texture. However, polycrystals cannot generally be considered as being mechanically elastically isotropic, even in the absence of crystallographic texture.

An example for the occurrence of macroscopic elastic anisotropy in the absence of crystallographic texture is provided by thin films, which can exhibit mechanical transverse isotropy owing to their microstructure and reduced dimensionality [10, 11]. A body is said to be mechanically elastically transversely isotropic, if the mechanical elastic constants exhibit rotational symmetry with respect to a particular symmetry axis (the specimen normal in the case considered here). Only recently, it has been demonstrated theoretically and experimentally by van Leeuwen *et al.* [10] that the occurrence of anisotropic grain-interaction is compatible with macroscopic elastic anisotropy even in the absence of crystallographic texture (see also Leoni *et al.* [12]). The notion ‘direction-dependent grain interaction’ (i.e. ‘anisotropic grain interaction’) signifies that different grain-interaction assumptions prevail along different directions in the specimen. Consider as an example the so-called Vook–Witt model adapted to diffraction stress analysis by van Leeuwen *et al.* [10] (see also Vook and Witt [13]). Here, a Reuss-type grain interaction is adopted perpendicular to the film surface (i.e. the stress tensor components perpendicular to the surface are identical for all crystallites), whereas a Voigt-type grain interaction is adopted for (all) directions within the plane of the film (i.e. the strain tensor components parallel to the surface are identical for all crystallites). The Vook–Witt grain-interaction assumptions thus represent extreme assumptions for the in-plane directions and for the direction perpendicular to the surface of the film. For this reason, the Vook–Witt model will, in general, not be able to describe the true elastic behaviour of a real thin film. To overcome this problem, the so-called inverse Vook–Witt model has been recently introduced by Welzel *et al.* [14] (see also Welzel *et al.* [15]) and it can be made likely that the four extreme models. Vook–Witt, inverse Vook–Witt, Reuss and Voigt, define bounds for true grain interaction in polycrystalline solids. Hence, the construction of an effective grain-interaction models has been proposed as a linear combination of the Reuss, Voigt, Vook–Witt and inverse Vook–Witt models [14].

Surface anisotropy was considered by Stickforth [11] as a source of macroscopic elastic anisotropy: the elastic behaviour of crystallites adjacent to the surface of a (bulk) polycrystal can be different from the elastic behaviour of crystals at some distance from the surface. In the bulk of a polycrystal, each crystallite is surrounded by other crystallites in three dimensions, whereas crystallites located at the surface of a polycrystal have no neighbouring crystallites in the direction perpendicular to the surface. Thus, for the crystallites adjacent to the surface not all directions are equivalent for the interaction of the grains.

Polycrystals with a grain-shape (morphological) texture provide another possible example for the occurrence of macroscopic elastic anisotropy (i.e. already in the absence of crystallographic texture). The grain-interaction in this case can be modelled by employing an extension of the Eshelby–Kröner grain-interaction model [16–18]. Whereas spherical grains (inclusions) have been considered in the traditional Eshelby–Kröner model, a procedure for the calculation of mechanical

and diffraction elastic constants involving ellipsoidal grains with their principal directions aligned along common axes in the specimen frame of reference has been developed for the case of an ideal grain-shape texture; for details, see Koch *et al.* [18]. It has to be stressed that it is the preferential morphological alignment of non-spherical grains that induces the macroscopic elastic anisotropy. Obviously, a polycrystal consisting of non-spherical grains with a random distribution of their shape orientations will be macroscopically elastically isotropic.

Both the Vook–Witt and inverse Vook–Witt models for surface anisotropy and the Eshelby–Kröner model for the case of grain-shape anisotropy involve direction-dependent (anisotropic) grain-interaction constraints. Thus, a comparative study of these models suggests itself. It will be shown here that similarities can be observed between the Vook–Witt and inverse Vook–Witt results on the one hand and the Eshelby–Kröner results on the other hand. This is remarkable, recognizing that the origin of a morphological texture has no relation with the origin of surface anisotropy. It will be demonstrated by both numerical and analytical calculations that the Eshelby–Kröner model becomes (approximately, to different degrees of accuracy) equivalent to the Vook–Witt and inverse Vook–Witt models in the limits of flat-disc shaped grains oriented parallel to the surface and needle-shaped grains oriented perpendicular to the surface, respectively. This can greatly simplify numerical algorithms for the calculation of elastic (and possibly plastic) grain interaction.

## 2. Theoretical background

### 2.1. Definitions

**2.1.1 Frames of reference.** Stresses, strains, and elastic constant are tensorial quantities and it is thus necessary to define frames of reference. It is convenient for the considerations presented in the following to use three Cartesian frames of reference: The crystal frame of reference ( $C$ ), the specimen frame of reference ( $S$ ) and the laboratory frame of reference ( $L$ ). For details on the definition of these frames of reference, see, for example, Welzel *et al.* [15] (for the definition of the crystal frame of reference in the case of non-cubic crystallites, see also Giacomazzo *et al.* [19]). In the following, a superscript ( $C$ ,  $S$  or  $L$ ) indicates the reference frame adopted for the representation of the reference frame used for tensor representation, but the same reference frame has to be adopted for all tensors in the equation. The relative orientation of the specimen frame of reference with respect to the laboratory frame of reference is given by the angles  $\psi$  and  $\varphi$ , where  $\psi$  is the inclination angle of the sample surface normal with respect to the diffraction vector (aligned along the  $L_3$  axis) and  $\varphi$  denotes the rotation of the sample around the sample surface normal (see also figure 1).

Rotation matrices can perform transformations of tensors from one to another frame of reference. For a detailed description of the rotation matrices required for performing the calculations described in this paper, see Leoni *et al.* [12] for the case of cubic crystal symmetry and consider the Appendix of Koch *et al.* [18] for cases of lower crystal symmetry. For a general introduction to the use of transformation matrices, see for example Hauk [1].

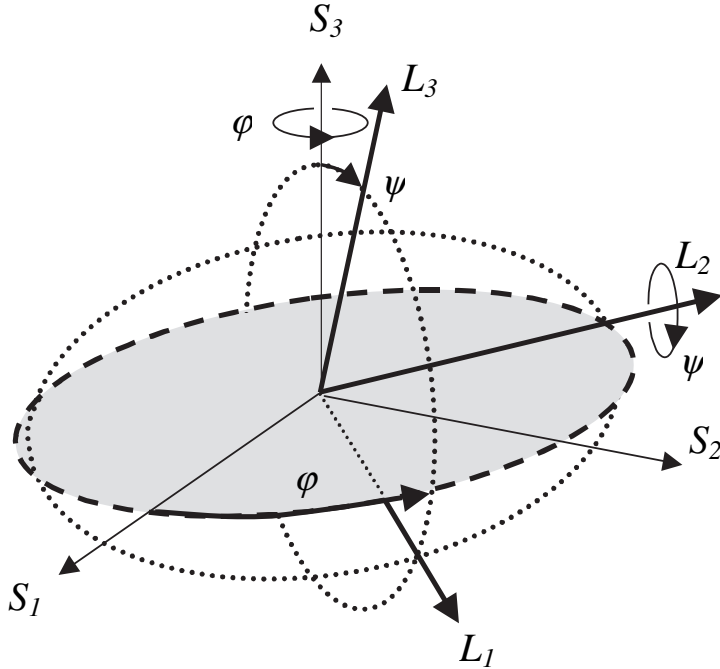


Figure 1. Definition of and relations between the sample ( $S$ ) and laboratory ( $L$ ) frames of reference.  $\psi$  is the inclination angle of the sample surface normal ( $S_3$  axis) with respect to the diffraction vector ( $L_3$  axis) and  $\varphi$  denotes the rotation of the sample around the sample surface normal.

**2.1.2 Definition of tensor averages.** In the following, it is useful to distinguish three types of averages of a tensor  $\Omega$  (to be identified as for example the strain tensor  $\epsilon$ ).

- (i) Averages of a tensor over all grains with a particular crystallographic orientation in the volume considered: this average will be denoted by the symbol  $\Omega(\mathbf{g})$ , where  $\mathbf{g}$  represents a vector in the three-dimensional crystallographic orientation (Euler) space  $G$  and defines the crystallographic orientation,  $\mathbf{g} = (\alpha, \beta, \gamma)^T$ , where  $\alpha$ ,  $\beta$  and  $\gamma$  are the three Euler angles. The convention of Roe and Krigbaum [20] for the definition of the Euler angles is adopted (see also Leoni *et al.* [12]).
- (ii) Averages over diffracting grains: a diffraction line contains data on only a subset of (generally non-connected) crystallites for which the diffracting planes are perpendicular to the chosen measurement direction (=direction of the diffraction vector). For a  $hkl$  diffraction line, the group of diffracting crystallites is selected by specifying the  $hkl$  of the reflection considered and the orientation of the diffraction vector with respect to the specimen reference frame, which can be identified by the angles  $(\varphi, \psi)$ . Therefore the sub  $(\varphi, \psi)$  and superscripts  $(hkl)$  are attached to the corresponding average denoted by braces,  $\{\Omega\}_{\varphi, \psi}^{hkl}$ . For details, see Leoni *et al.* [12].
- (iii) Averages over all crystallographically differently oriented grains in the volume considered: this average will be denoted by angular brackets,  $\langle \Omega \rangle$ , and can be

calculated as follows:

$$\langle \boldsymbol{\Omega} \rangle = \frac{1}{8\pi^2} \int_G \boldsymbol{\Omega} d^3 \mathbf{g}. \quad (1)$$

The factor  $1/8\pi^2$  serves as a normalization factor and is the volume of the Euler space  $G$ .

**2.1.3 Grain-shape/morphological texture.** For the calculation of mechanical and diffraction elastic constants of polycrystals with a grain-shape texture, the treatment will be restricted to polycrystals consisting of ellipsoidal grains. Of course, a real polycrystal cannot consist of ellipsoidal grains (only). The ellipsoidal shape is an idealized shape, which is adopted in order to represent grains with (average) aspect ratios different from one, whereas a spherical shape is adopted for grains with an (average) aspect ratio of one. It is assumed that the ellipsoidal grains exhibit identical orientations of their principal (shape) axes in the specimen frame of reference, i.e. the ellipsoidal grains are aligned along common axes (an ideal grain-shape texture occurs). An ideal grain-shape texture is considered because only in this case unique mechanical elastic constants and diffraction stress factors can be calculated employing the Eshelby–Kröner model (for a more detailed discussion of the effect of a non-ideal morphological texture, see Koch *et al.* [18]).

Note that the principal axes of a grain, as meant here, are only related to the *external* (geometrical) shape of the grain. Thereby nothing is prescribed regarding the crystallographic orientation of the grain (crystallite). In general, the (ellipsoidal) grains constituting the specimen will have different crystallographic orientations.

The shape of the grains is described by a shape parameter  $\eta$ , which is defined as the ratio of the length of the principal axis of the ellipsoid in the  $S_3$ -direction ( $a_3$ ) of the specimen frame of reference to the length of the principal axes of the ellipsoid in the  $S_1$ -direction ( $a_1$ ) and the  $S_2$ -direction ( $a_2$ ) in the specimen frame of reference:

$$\eta = \frac{a_3}{a_1} = \frac{a_3}{a_2} \quad (2)$$

Thus, the considered ellipsoidal grains present rotational shape symmetry with respect to the surface normal of the specimen.

**2.1.4 Mechanical elastic constants.** The Vook–Witt and inverse Vook–Witt models were initially developed for the case of a plane, rotationally symmetric state of mechanical stress/strain. Such loading states are frequently met in thin films [15]:

$$\langle \boldsymbol{\varepsilon}^S \rangle = \begin{pmatrix} \varepsilon_{||}^S & 0 & 0 \\ 0 & \varepsilon_{||}^S & 0 \\ 0 & 0 & \varepsilon_{\perp}^S \end{pmatrix}, \quad (3)$$

$$\langle \boldsymbol{\sigma}^S \rangle = \begin{pmatrix} \sigma_{||}^S & 0 & 0 \\ 0 & \sigma_{||}^S & 0 \\ 0 & 0 & 0 \end{pmatrix}. \quad (4)$$

Under these loading conditions two mechanical elastic constants A and B suffice, as only three independent non-zero stress and strain tensor components occur:

$$\varepsilon_{||}^S = A\sigma_{||}^S, \quad (5)$$

$$\varepsilon_{\perp}^S = B\sigma_{||}^S. \quad (6)$$

**2.1.5 Diffraction (X-ray) stress factors.** The  $\varphi$ , and  $hkl$ -dependent diffraction stress factors  $F_{ij}(\psi, \varphi, hkl)$  relate the diffraction strain  $\{\varepsilon_{33}^L\}_{\varphi, \psi}^{hkl}$  measured for an  $hkl$  reflection at a specimen tilt angle  $\psi$  and rotation angle  $\varphi$  to the mechanical stress tensor expressed in the specimen frame of reference  $\langle \sigma^S \rangle$  (see Welzel and Mittemeijer [2]; the Einstein convention, i.e. summation over indices appearing twice in a formula, is adopted throughout the paper):

$$\{\varepsilon_{33}^L\}_{\varphi, \psi}^{hkl} \equiv \varepsilon_{\varphi, \psi}^{hkl} = F_{ij}(\psi, \varphi, hkl) \langle \sigma_{ij}^S \rangle. \quad (7)$$

In the following, the abbreviation introduced with the first equality (identity) in equation (7) will be used to denote the diffraction strain. Note that the  $F_{ij}(\psi, \varphi, hkl)$  are not components of a tensor since they relate the lattice strain (a scalar) to the stress tensor (expressed in the  $S$ -system).

For the case of a plane, rotationally symmetric state of stress (cf. equations (3) and (4)) equation (7) can be simplified to:

$$\varepsilon_{\varphi, \psi}^{hkl} = (F_{11}(\psi, \varphi, hkl) + F_{22}(\psi, \varphi, hkl)) \sigma_{||}^S. \quad (8)$$

For the case of transverse elastic isotropy and under a plane, rotationally symmetric state of stress, the diffraction strain is independent of the angle  $\varphi$ , thus,  $\varphi$  can be arbitrarily set to zero (or any other value) for the diffraction stress factors and  $\varphi$  as an index can be suppressed for the diffraction strain:

$$\varepsilon_{\psi}^{hkl} = (F_{11}(\psi, 0, hkl) + F_{22}(\psi, 0, hkl)) \sigma_{||}^S. \quad (9)$$

For the case that the specimen is macroscopically elastically isotropic, the diffraction (X-ray) elastic constants  $S_1^{hkl}$  and  $(1/2)S_2^{hkl}$  can be used instead of the diffraction (X-ray) stress factors. The diffraction (X-ray) elastic constants depend on the reflection  $hkl$ , but they *do not* depend upon  $\varphi$  and  $\psi$ . The relation between the diffraction (X-ray) stress factors and the diffraction (X-ray) elastic constants for *macroscopically elastically isotropic specimens* reads (see, for example, Hauk, [1]):

$$F_{ij}(\psi, \varphi, hkl) = \frac{1}{2} S_2^{hkl} m_i^S m_j^S + S_1^{hkl} \delta_{ij}, \quad (10)$$

where  $\mathbf{m}^S$  is the normalized diffraction vector in the specimen frame of reference:

$$\mathbf{m}^S = \begin{pmatrix} \sin \psi \cos \varphi \\ \sin \psi \sin \varphi \\ \cos \psi \end{pmatrix}. \quad (11)$$

For macroscopically elastically isotropic specimens, equation (8) can be rewritten in terms of the diffraction (X-ray) elastic constants as:

$$\varepsilon_{\varphi}^{hkl} = 2S_1^{hkl} \sigma_{\parallel}^S + \frac{1}{2} S_2^{hkl} \sigma_{\parallel}^S \sin^2 \psi. \quad (12)$$

## 2.2. Thin films and surface anisotropy: the Vook–Witt and inverse Vook–Witt models

The calculation of mechanical elastic constants and diffraction stress factors on the basis of the Vook–Witt and inverse Vook–Witt models has been discussed in detail by Welzel *et al.* [14, 15]. The essentials relevant to this work will be briefly summarised in the following.

**2.2.1 The Vook–Witt model.** In a thin film (with a columnar microstructure) or in any case for solids adjacent to the surface, in contrast with bulk specimens, each crystallite is surrounded by neighbouring crystallites in only two dimensions. The interaction between the crystallites (columns) in a direction perpendicular to the surface (of the film) can be weak (there are often voids at the grain boundaries in thin films) and thus, the grain interaction cannot be the same for the inplane directions and the direction perpendicular to the surface. Grain-interaction assumptions under a plane, rotationally symmetric state of stress (cf. equations (3) and (4)) may then be formulated as follows: (i) the strain parallel to the surface is rotationally symmetric and (ii) equal for all crystallites and (iii) the stresses perpendicular to the surface are zero for all crystallites, i.e. the crystallites can deform freely in this direction. These assumptions fix parts of the stress and strain tensors for all crystallites, recognizing the symmetry of the stress and strain tensors:

$$\boldsymbol{\varepsilon}^S = \begin{pmatrix} \varepsilon_{\parallel}^S & 0 & \diamond \\ 0 & \varepsilon_{\parallel}^S & \diamond \\ \diamond & \diamond & \diamond \end{pmatrix}, \quad (13)$$

$$\boldsymbol{\sigma}^S = \begin{pmatrix} \diamond & \diamond & 0 \\ \diamond & \diamond & 0 \\ 0 & 0 & 0 \end{pmatrix} \quad (14)$$

The tensor components marked by  $\diamond$  are not explicitly specified for every crystallite, but these components can be calculated from Hooke’s law for every crystallite as follows:

$$\varepsilon_{ij}^S = s_{ijkl}^S \sigma_{kl}^S. \quad (15)$$

The  $s_{ijkl}^S$  are the single crystal elastic compliances expressed in the specimen frame of reference. Equation (15) represents a system of nine equations for eighteen unknown, but as the strain and stress tensors are symmetric (i.e.  $\varepsilon_{ij} = \varepsilon_{ji}$  and  $\sigma_{ij} = \sigma_{ji}$ ), equation (15) is a short notation for six independent equations for twelve independent unknowns. If six components of the twelve unknowns are known, as a consequence, the other components can be calculated by solving the system of equations (15). Adopting the Vook–Witt model (cf. equations (13) and (14)), six stress and strain tensor components are set equal to the corresponding mechanical

values for all crystallites and thus, the remaining six unknown tensor components can be calculated from the system of equation (15). The elastic constants A and B can be calculated from (cf. equations (5) and (6)):

$$A = \frac{\varepsilon_{\parallel}^S}{\sigma_{\parallel}^S} = \frac{\langle \varepsilon_{11}^S \rangle}{\langle \sigma_{11}^S \rangle} \quad (16)$$

and

$$B = \frac{\varepsilon_{\perp}^S}{\sigma_{\parallel}^S} = \frac{\langle \varepsilon_{33}^S \rangle}{\langle \sigma_{11}^S \rangle}. \quad (17)$$

The sum of the two stress factors relevant for the loading state considered (cf. equations (3) and (4)) follows from equations (9):

$$(F_{11}(\psi, 0, hkl) + F_{22}(\psi, 0, hkl)) = \frac{\varepsilon_{\psi}^{hkl}}{\sigma_{\parallel}^S}. \quad (18)$$

**2.2.2 The inverse Vook–Witt model.** The inverse Vook–Witt model has been introduced on the basis of a ‘symmetry’ consideration for extreme material behaviour: Reuss vs. Voigt and Vook–Witt vs. inverse Vook–Witt. Thus, the inverse Vook–Witt model is essential for the construction of an effective grain-interaction model for thin films and surface adjacent material of bulk solids. The inverse Vook–Witt model was originally proposed by Welzel *et al.* [14]. The grain-interaction assumptions for this model are as follows: (i) the in-plane stress (parallel to the surface) is rotationally symmetric and (ii) equal for all crystallites and (iii) the strain perpendicular to the surface is equal for all crystallites. Like in the Vook–Witt model, these assumptions fix certain strain and stress tensor components for all crystallites, recognising the symmetry of the stress and strain tensors (cf. equations (13) and (14)); note that grain-interaction assumptions of this type have been proposed in a different context for composites; see Tsai and Hahn [21]):

$$\boldsymbol{\varepsilon}^S = \begin{pmatrix} \diamond & \diamond & 0 \\ \diamond & \diamond & 0 \\ 0 & 0 & \varepsilon_{\perp}^S \end{pmatrix}, \quad (19)$$

$$\boldsymbol{\sigma}^S = \begin{pmatrix} \sigma_{\parallel}^S & 0 & \diamond \\ 0 & \sigma_{\parallel}^S & \diamond \\ \diamond & \diamond & \diamond \end{pmatrix}. \quad (20)$$

The missing strain and stress tensor components for each crystallite, marked by  $\diamond$ , can be calculated by solving the system of equations (15) (cf. above discussion for the Vook–Witt model).

For the calculation of the mechanical elastic constants, A and B, it is necessary to assure that  $\sigma_{\perp}^S = \langle \sigma_{33}^S \rangle$  is zero (with the Vook–Witt approach this is inherently the case as this has been realized by the boundary conditions). To this end, a procedure as described in Welzel *et al.* [14] can be followed. When it has been realized that  $\sigma_{\perp}^S$  is zero for a given combination of  $\sigma_{\parallel}^S$  and  $\varepsilon_{\perp}^S$ , the elastic constants A and B can be calculated from equations (16) and (17). The sum of the two stress factors relevant

for the loading state considered (cf. equations (3) and (4)) follows from equation (9) (cf. also section 2.1).

### 2.3. The Eshelby–Kröner model – the case of a grain-shape texture

In order to calculate the elastic constants of a polycrystal from single-crystal data according to the approach by Eshelby [7] and Kröner [8], the crystallites surrounding a considered individual grain in a polycrystal are conceived as an elastically homogeneous matrix with the elastic properties of the *entire* polycrystal. The elastic constants of the polycrystal are determined by the calculation of the stresses and strains of an inclusion (a grain) embedded in the homogeneous matrix (the polycrystal). Traditionally, a spherical shape of the inclusion is considered [8]. It goes without saying that the Eshelby–Kröner model based on a spherical inclusion will only work for polycrystals consisting of (on the average) spherical, equi-axed grains.

The effect of an ideal grain-shape (morphological) texture on mechanical and diffraction elastic constants can be considered in the Eshelby–Kröner model by considering ellipsoidal inclusions with their principal axes aligned along common directions in the specimen frame of reference. For characterizing the grain-shape texture, the convention introduced in section 2.1 (Grain-shape/morphological texture) will be adopted. For a detailed outline of the calculation and a thorough discussion of results, the reader is referred to Koch *et al.* [18]. The essentials relevant for the following will be briefly summarized here.

In the Eshelby–Kröner model, the strain  $\boldsymbol{\varepsilon}$  in the considered crystallite (inclusion) can be calculated from the mechanical strain  $\langle \boldsymbol{\varepsilon} \rangle$  via the tensor  $\boldsymbol{\Phi}$  as follows:

$$\boldsymbol{\varepsilon}(\alpha, \beta, \gamma) = (\mathbf{u}(\alpha, \beta, \gamma) + \mathbf{I})\langle \boldsymbol{\varepsilon} \rangle = \boldsymbol{\Phi}(\alpha, \beta, \gamma)\langle \boldsymbol{\varepsilon} \rangle, \quad (21)$$

where  $\mathbf{I}$  is the rank-four identity.  $\boldsymbol{\Phi}$  has sometimes been called strain-localization tensor (see, for example, Moudon and Molinari [22]; use of this name should not be promoted, as the indication ‘strain-localization tensor’ is misleading). The tensor  $\mathbf{u}$  depends on the mechanical, macroscopic elastic stiffness tensor  $\mathbf{C}$ , the single-crystal elastic constants of the grain considered  $\mathbf{c}$  and the so-called Morris tensor  $\mathbf{E}$  (see below):

$$\mathbf{u}(\alpha, \beta, \gamma) = [\mathbf{E}(\mathbf{c}(\alpha, \beta, \gamma) - \mathbf{C}) + \mathbf{I}]^{-1} - \mathbf{I}. \quad (22)$$

The orientation dependence of  $\mathbf{u}$  originates from the orientation dependence of  $\mathbf{c}$ . The Morris tensor  $\mathbf{E}$  can be calculated for the case of an ellipsoidal grain (inclusion) shape as follows [23, 24]:

$$E_{ijmn} = \frac{a_1 a_2 a_3}{8\pi} \int_0^\pi d\theta \sin \theta \int_0^{2\pi} d\phi \frac{D_{ij}^{-1}(\mathbf{k}) k_j k_n + D_{jk}^{-1}(\mathbf{k}) k_i k_j}{((a_1 k_1)^2 + (a_2 k_2)^2 + (a_3 k_3)^2)^{3/2}} \quad (23)$$

where the  $a_i$  are the lengths of the principal axes of the ellipsoid (see section 2) and

$$D_{ik} = C_{jkn} k_j k_m. \quad (24)$$

$\mathbf{C}$  is the elastic stiffness tensor of the matrix (polycrystal, see above). The  $k_i$  can be expressed in terms of the two spherical co-ordinates  $\varphi$  and  $\psi$  as:

$$k_1 = \sin \psi \cos \varphi, \quad (25)$$

$$k_2 = \sin \psi \sin \varphi, \quad (26)$$

$$k_3 = \cos \psi. \quad (27)$$

It should be noted that, strictly speaking,  $E_{ijmn}$  should be written as  $E_{ijmn}^G$ , where  $G$  is a frame of reference defined by the principal axes of the ellipsoid. Due to the definition of the orientation of the ellipsoid (see section 2), the frame of reference  $G$  coincides with the frame of reference  $S$ . The stiffness tensor  $\mathbf{C}$  has to be expressed in the frame of reference  $S$  for practical calculations. Thus, according to equation (23), the effect induced by a morphological texture on the local strain is described by the Morris tensor  $\mathbf{E}$ .

The macroscopic, mechanical elastic constants can be determined as follows. Calculating the mechanical average strain  $\varepsilon$  by adopting equation (21) for each grain in the specimen implies that

$$\langle \Phi(\alpha, \beta, \gamma) \rangle = \mathbf{I}. \quad (28)$$

Thus, it holds that

$$\langle \mathbf{u}(\alpha, \beta, \gamma) \rangle = 0. \quad (29)$$

Equation (29) defines implicitly the mechanical stiffness tensor ( $\mathbf{C}$ , or compliance tensor  $\mathbf{S}$ ) of the polycrystal: the tensorial equation (29) can be considered as a set of scalar equations, where the unknowns are the components of the mechanical stiffness tensor. It has to be noted that  $\langle \mathbf{u} \rangle$  exhibits the same symmetries as  $\mathbf{C}$  (and  $\mathbf{S}$ ), i.e. the number of independent tensor components is equal (e.g. only two independent components occur for a macroscopically elastically isotropic polycrystal). Equation (29) is thus a short notation for a set of  $N$  independent (scalar) equations containing  $N$  independent components of the mechanical stiffness (or compliance) tensor. Only in rare cases, the (sets of) equations can be solved for the (components of the) stiffness or compliance tensors explicitly. Generally, numerical iterative procedures are required. A detailed outline of the calculation scheme can be found in Koch *et al.* [18].

The diffraction stress factors can be calculated from (see equations (41)–(44) in Koch *et al.* [18]):

$$F_{op}(\varphi, \psi, hkl) = \frac{\int_0^{2\pi} (S_{ijop}^S + t_{ijop}^S(hkl, \varphi, \psi, \lambda)) f^*(hkl, \varphi, \psi, \lambda) d\lambda}{\int_0^{2\pi} f^*(hkl, \varphi, \psi, \lambda) d\lambda} m_i^S m_j^S, \quad (30)$$

where

$$t_{ijkl}(\alpha, \beta, \gamma) = u_{ijmn}(\alpha, \beta, \gamma) S_{mnkl}. \quad (31)$$

Note that to calculate  $F_{ij}(\varphi, \psi, hkl)$  the mechanical elastic constants,  $S_{ijkl}^S$ , have to be calculated first, employing the above mentioned procedure.

### 3. Comparison of the Vook–Witt and the inverse Vook–Witt models with the Eshelby–Kröner model

#### 3.1. Diffraction stress analysis

The Vook–Witt (VW) model, the inverse Vook–Witt (iVW) model, by forcing specific strain and stress components to be equal for all crystallites, and the Eshelby–Kröner (EK) model, by adopting a grain-shape (morphological) texture, are direction-dependent grain-interaction models. They imply that a polycrystal is macroscopically elastically anisotropic even in the absence of crystallographic texture. This macroscopic elastic anisotropy is revealed in diffraction-stress analysis by the occurrence of non-linear, instead of linear,  $\sin^2 \psi$ -plots (even in the absence of shear stresses; see Welzel *et al.* [14, 15, 25]).

The  $\sin^2 \psi$ -plots as calculated according to the VW and iVW models and the EK model (for morphological textures with  $\eta = 0.01$  and  $\eta = 100$ , cf. section 2), all for crystallographically untextured copper polycrystals subjected to a plane-rotationally symmetric state of stress ( $\sigma_{\parallel} = 100$  MPa), are shown in figure 2. Similarities can be observed between the VW and iVW results on the one hand and the EK results on the other hand. This is a remarkable observation, recognizing that the EK model expresses the effect of a morphological texture whereas the VW/iVW models are compatible with the occurrence of surface anisotropy. The VW model results in  $\sin^2 \psi$ -plots similar to those of the EK model for flat-disc shaped grains ( $\eta = 0.01$ ), whereas the  $\sin^2 \psi$ -plots obtained from the iVW model exhibit similarities (but less outspoken than for the VW model) with the corresponding plots obtained from the EK model for needle-shaped grains ( $\eta = 100$ ).

In the following it will be shown that such similarities do not only occur for  $\sin^2 \psi$ -plots (i.e. for the diffraction stress factors), but also for the mechanical,

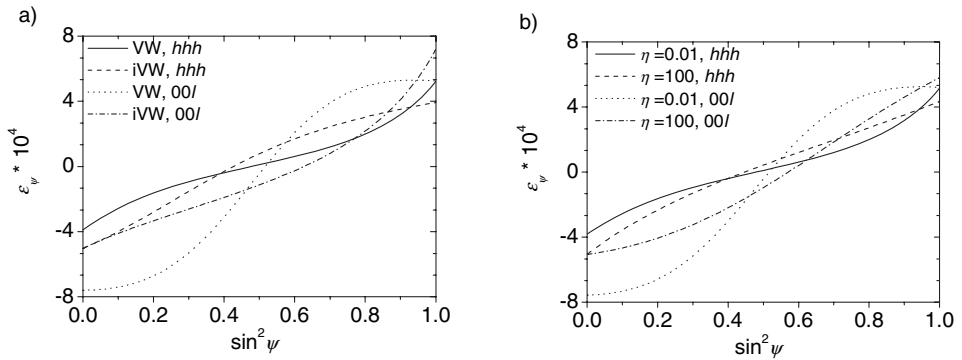


Figure 2.  $\sin^2 \psi$ -plots for the  $hhh$  and  $00l$  reflections of a crystallographically untextured copper polycrystal subjected to a plane-rotationally symmetric state of stress ( $\sigma_{\parallel} = 100$  MPa): (a) according to the Vook–Witt (VW) and inverse Vook–Witt (iVW) models; (b) according to the Eshelby–Kröner model for an ideal grain-shape texture involving different ellipsoidal crystallite morphologies (for single-crystal compliances of copper, set table 1).

Table 1. Single crystal elastic constants of copper [26]. The compliance matrix components  $s_{ij}$  have been given together with the anisotropy factor  $A_i = 2(s_{11}^C - s_{12}^C)/s_{44}^C$ . The Voigt two-index notation (see, for example, Hauk [1]) is used.

	$s_{11}(\text{TPa}^{-1})$	$s_{12}(\text{TPa}^{-1})$	$s_{44}(\text{TPa}^{-1})$	$A_i (\text{TPa}^{-1})$
Cu (fcc)	14.98	-6.29	13.26	3.21

macroscopic elastic constants, the variances of specific stress and strain-tensor components and for the distributions of stresses and strains in Euler space. Closed-form simplifications of the tensor  $\Phi$  (cf. equation (21)) will be presented in section 3.5, which demonstrate why such similarities do occur.

### 3.2. Mechanical elastic constants

The mechanical elastic constants  $\mathbf{A}$  and  $\mathbf{B}$  (cf. equations (5) and (6)), as calculated employing the EK model, are shown as functions of the grain-aspect ration  $\eta$  in figure 3 (line with open circles). The values of  $\mathbf{A}$  and  $\mathbf{B}$  for the VW and the iVW models as well as for the Reuss (R) and Voigt (V) models have been indicated too. It can be observed that the values of  $\mathbf{A}$  and  $\mathbf{B}$  calculated according to the EK model depend on the grain shape (for the grains-shape texture considered here) and fall between the VW and iVW values calculated for the same material. As the grain shape approaches the limit of a flat-disc shaped grains ( $\eta \rightarrow 0$ ),  $\mathbf{A}$  and  $\mathbf{B}$  tend to the corresponding VW values, whereas in the limit of needle-shaped grains ( $\eta \rightarrow \infty$ ),  $\mathbf{A}$  and  $\mathbf{B}$  tend towards the corresponding iVW values, but much less outspokenly as for the VW values for  $\eta \rightarrow 0$ :

$$\lim_{\eta \rightarrow 0} \mathbf{A}_{EK} \approx \mathbf{A}_{VW}, \quad (32)$$

$$\lim_{\eta \rightarrow 0} \mathbf{B}_{EK} \approx \mathbf{B}_{VW}, \quad (33)$$

$$\lim_{\eta \rightarrow \infty} \mathbf{A}_{EK} \rightarrow \mathbf{A}_{iVW}, \quad (34)$$

$$\lim_{\eta \rightarrow \infty} \mathbf{B}_{EK} \rightarrow \mathbf{B}_{iVW}, \quad (35)$$

Subscripts have been attached to  $\mathbf{A}$  and  $\mathbf{B}$  in order to specify the grain-interaction model. The symbol ‘ $\approx$ ’ (‘approximately equal’) is used, instead of ‘=’, in order to express, that, within the investigated range of grain shapes for the case  $\eta \rightarrow 0$ , within numerical accuracy the values for  $\mathbf{A}$  and  $\mathbf{B}$  are equal to the values obtained using the VW model, for the same material. The symbol ‘ $\rightarrow$ ’ has been used for the case  $\eta \rightarrow \infty$  in order to express that the values of  $\mathbf{A}$  and  $\mathbf{B}$  approach the values obtained using the iVW model for the same material, but still differ significantly.

It was shown by Hill [6] that the mechanical elastic constants calculated according to the Reuss and Voigt models provide absolute bounds for the possible elastic behaviour of a polycrystal. The results obtained for the mechanical elastic constants

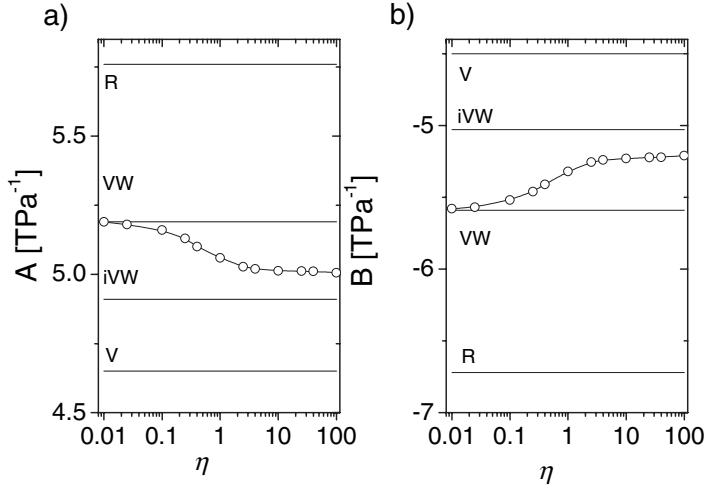


Figure 3. The macroscopic, mechanical elastic constants A and B of a crystallographically untextured copper polycrystal (see equations (5) and (6)) according to the Vook–Witt (VW), inverse Vook–Witt (iVW) and the Eshelby–Kröner model for an ideal grain-shape texture, as a function of the grain aspect ratio  $\eta$  (line with open circles). For comparison, the values for A and B according to the Reuss (R) and Voigt (V) models have also been indicated (for single-crystal compliances of copper, see table 1).

A and B from the VW, iVW and EK models accordingly fall in between the Reuss and Voigt values (see figure 3).

### 3.3. Variances of stress and strain components

The variance of a tensor  $\mathbf{\Omega}$  will be denoted by square brackets  $[\mathbf{\Omega}^2]$  and can be calculated as follows

$$[\mathbf{\Omega}^2] = \frac{1}{8\pi^2} \int_G (\mathbf{\Omega} - \langle \mathbf{\Omega} \rangle)^2 d^3g. \quad (36)$$

Obviously it holds for the VW model (cf. equations (13) and (14)):

$$[(\varepsilon_{11}^S)^2]_{\text{VW}} = [(\varepsilon_{22}^S)^2]_{\text{VW}} \equiv 0 \quad (37)$$

and

$$[(\sigma_{33}^S)^2]_{\text{VW}} \equiv 0, \quad (38)$$

and similarly for the iVW model (cf. equations (19) and (20)):

$$[(\sigma_{11}^S)^2]_{\text{iVW}} = [(\sigma_{22}^S)^2]_{\text{iVW}} \equiv 0 \quad (39)$$

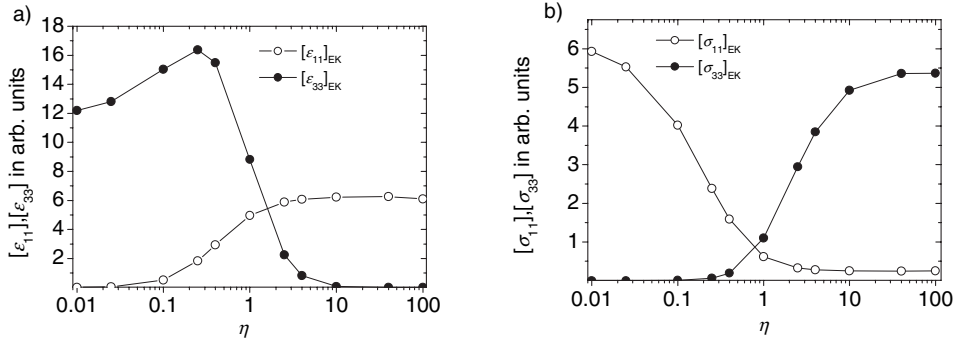


Figure 4. Variances (cf. equation (36)) of specific stress- and strain-tensor components calculated employing the EK model for an ideal grain-shape texture as a function of the grain aspect ratio  $\eta$  of a crystallographically untextured copper polycrystal. (a) Variances of the strain tensor components  $\varepsilon_{11}^S$  and  $\varepsilon_{33}^S$ . (b) Variances of the stress tensor components  $\sigma_{11}^S$  and  $\sigma_{33}^S$ . For all calculations, a plane, rotationally symmetric state of mechanical stress with  $\sigma_{11}^S = 100$  MPa has been imposed (for single-crystal compliances of copper, see table 1).

and

$$\left[ (\varepsilon_{33}^S)^2 \right]_{\text{iVW}} \equiv 0. \quad (40)$$

The variances of the tensor components  $\varepsilon_{11}^S$ ,  $\varepsilon_{33}^S$ ,  $\sigma_{11}^S$  and  $\sigma_{33}^S$  as calculated employing the EK model are presented in figure 4 as a function of the grain aspect ratio  $\eta$  (lines with open and closed circles). Comparing the results shown in figure 4 with the identities (37)–(40), it can be observed that the grain-interaction constraints of the EK model approach the VW constraints for  $\eta \rightarrow 0$  and the iVW constraints for  $\eta \rightarrow \infty$ :

$$\lim_{\eta \rightarrow 0} \left[ (\varepsilon_{11}^S)^2 \right]_{\text{EK}} \approx 0, \quad (41)$$

$$\lim_{\eta \rightarrow 0} \left[ (\sigma_{33}^S)^2 \right]_{\text{EK}} \approx 0, \quad (42)$$

$$\lim_{\eta \rightarrow \infty} \left[ (\sigma_{11}^S)^2 \right]_{\text{EK}} \rightarrow 0, \quad (43)$$

$$\lim_{\eta \rightarrow \infty} \left[ (\varepsilon_{33}^S)^2 \right]_{\text{EK}} \approx 0. \quad (44)$$

It is worth noting that the similarities with the EK model occur much less obviously for the case of the iVW model (for  $\eta \rightarrow \infty$ ) than for the VW model (for  $\eta \rightarrow 0$ ): the variance of the stress tensor component  $\sigma_{11}^S$  still differs significantly from zero. This has been indicated by using the symbol ‘ $\rightarrow$ ’ instead of the symbol ‘ $\approx$ ’ in equation (43).

### 3.4. Strain contours in Euler space

So far, average quantities, like diffraction and mechanical elastic constants, have been employed for comparing the grain-interactions prescribed by the VW, iVW and EK models. A sensitive way to investigate (non)similarities in the grain-interaction is provided by local inspection of the Euler space  $G$ . Thus, contour plots for the strain-tensor component  $\varepsilon_{11}^s$  calculated according to different grain-interaction models in the section  $\alpha=0$  of Euler space  $G$  are shown in figure 5.

Results for the EK model with  $\eta=0.1$  and  $\eta=1$  are shown in figures 5a and 5b. Evidently, decreasing  $\eta$  decreases the extent of strain variation which is compatible with approaching the VW model for which  $\varepsilon_{11}^s$  is constant. Increasing  $\eta$  (cf. figures 5b and 5c) leads to results resembling those obtained for the iVW model shown in figure 5d.

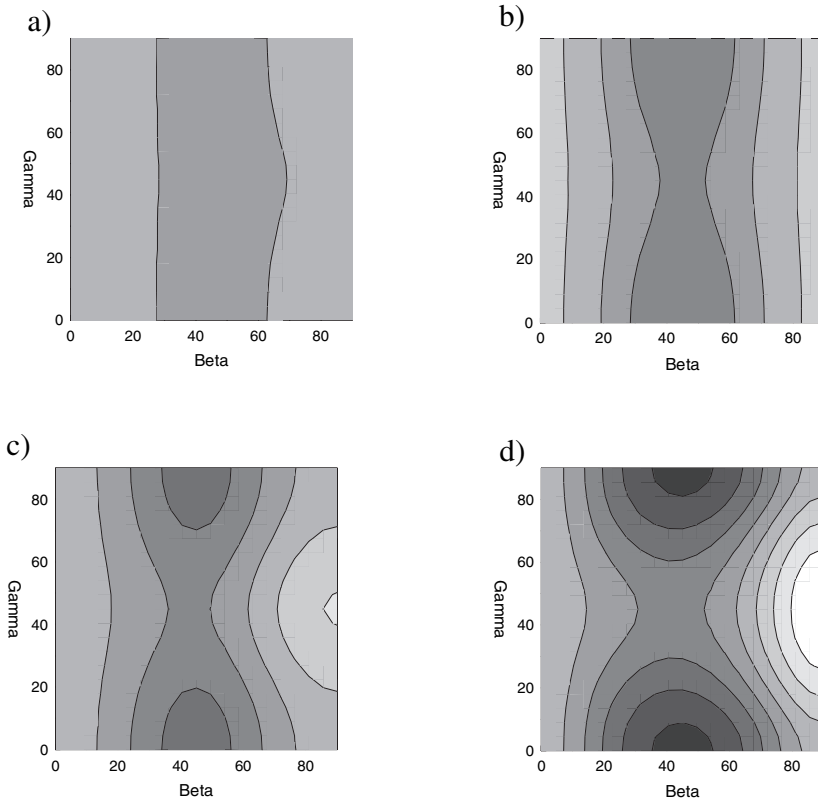


Figure 5. Contour plots for the strain-tensor component  $\varepsilon_{11}^s$  of crystallographically untextured copper polycrystal calculated according to different grain-interaction models in the section  $\alpha=0$  of the orientation, Euler space  $G$ : for an ideal grain-shape texture with  $\eta=0.1$  (a),  $\eta=1$  (b),  $\eta=10$  (c) and inverse Vook–Witt model (d). For all calculations, a plane, rotationally symmetric state of mechanical stress with  $\sigma_{11}^i = 100$  MPa has been imposed (for single-crystal compliances, see table 1). Ten contour levels in the strain range from 0 (black) to  $0.85 \times 10^{-3}$  (white) have been used.

Similar results were obtained for other strain and stress components and for other sections of Euler space.

### 3.5. Analytical simplifications of the Eshelby–Kröner model for limiting grain shapes

So far, the VW, iVW and EK models have been compared on the basis of numerical calculations. The results obtained have suggested that the EK model for the ideal grain-shape texture considered here approaches the VW model for  $\eta \rightarrow 0$  and the iVW model for  $\eta \rightarrow \infty$ . Hence it is attempted in this section to arrive at analytical approximations of the tensor  $\Phi$  (cf. equation (21)) in the limits  $\eta \rightarrow 0$  and  $\eta \rightarrow \infty$ . On that basis identification of effective grain-interaction assumptions concerning the strain tensor can be made using equation (21). Analogously, grain-interaction assumptions concerning the stress tensor can in principle be made using (cf. equations (15) and (21))

$$\sigma(\alpha, \beta, \gamma) = \mathbf{c}(\alpha, \beta, \gamma) \Phi(\alpha, \beta, \gamma) \langle \varepsilon \rangle. \quad (45)$$

However, even if analytical results for  $\Phi$  are available, analytical simplifications of equation (45) are not feasible in general, as  $\mathbf{c}(\alpha, \beta, \gamma)$  generally has only non-zero components. Thus, grain-interaction assumptions concerning stress tensor components cannot be easily identified. The reason for this (seeming) in-equivalence of the stress and strain tensors with respect to the identification of grain-interaction assumptions is a consequence of the formulation of Eshelby’s Gedanken experiment [7], which is the basis for the derivation of equation (21), in terms of strains. In principle, the character of the stress and strain tensors with respect to a straightforward identification of grain-interaction assumptions would have been reversed, had Eshelby’s Gedanken experiment been formulated in terms of stresses instead of strains.

**3.5.1 The limit of flat-disc shaped grains.** The following analytical simplification of  $\Phi$  can be obtained in the limit of flat-disc shaped grains ( $\eta \rightarrow 0$ ; for the details of the derivation, see Appendix):

$$\lim_{n \rightarrow 0} \Phi = \begin{bmatrix} 1 & 0 & 0 & 0 & 0 & 0 \\ 0 & 1 & 0 & 0 & 0 & 0 \\ \Phi_{31} & \Phi_{32} & \Phi_{33} & \Phi_{34} & \Phi_{35} & \Phi_{36} \\ \Phi_{41} & \Phi_{42} & \Phi_{43} & \Phi_{44} & \Phi_{45} & \Phi_{46} \\ \Phi_{51} & \Phi_{52} & \Phi_{53} & \Phi_{54} & \Phi_{55} & \Phi_{56} \\ 0 & 0 & 0 & 0 & 0 & \Phi_{66} \end{bmatrix}. \quad (46)$$

Inserting equation (46) into equation (21), considering a planar, rotationally symmetric state of stress-strain (cf. equation (3)), results in the following form for the

strain tensor:

$$\boldsymbol{\varepsilon}^S = \begin{bmatrix} \varepsilon_{\parallel} & 0 & (\Phi_{51} + \Phi_{52})\varepsilon_{\parallel} + \Phi_{51}\varepsilon_{\perp} \\ 0 & \varepsilon_{\parallel} & (\Phi_{41} + \Phi_{42})\varepsilon_{\parallel} + \Phi_{43}\varepsilon_{\perp} \\ (\Phi_{51} + \Phi_{52})\varepsilon_{\parallel} + \Phi_{53}\varepsilon_{\perp} & (\Phi_{41} + \Phi_{42})\varepsilon_{\parallel} + \Phi_{43}\varepsilon_{\perp} & (\Phi_{31} + \Phi_{32})\varepsilon_{\parallel} + \Phi_{33}\varepsilon_{\perp} \end{bmatrix}. \quad (47)$$

Comparing equation (47) with equation (13) it follows that the grain-interaction in the EK model in the limit of flat-disc shaped crystallites leads to constraints for the strain tensor components compatible with those adopted in the VW model.

**3.5.2 The limit of needle-shaped grains.** The following analytical simplification of  $\Phi$  can be obtained in the limit of needle-shaped grains ( $\eta \rightarrow \infty$ ; for the details of the derivation, see Appendix):

$$\lim_{\eta \rightarrow \infty} \Phi = \begin{bmatrix} \Phi_{11} & \Phi_{12} & \Phi_{13} & \Phi_{14} & \Phi_{15} & \Phi_{16} \\ \Phi_{21} & \Phi_{22} & \Phi_{23} & \Phi_{24} & \Phi_{25} & \Phi_{26} \\ 0 & 0 & 1 & 0 & 0 & 0 \\ \Phi_{41} & \Phi_{42} & \Phi_{43} & \Phi_{44} & \Phi_{45} & \Phi_{46} \\ \Phi_{51} & \Phi_{52} & \Phi_{53} & \Phi_{54} & \Phi_{55} & \Phi_{56} \\ \Phi_{61} & \Phi_{62} & \Phi_{63} & \Phi_{64} & \Phi_{65} & \Phi_{66} \end{bmatrix}. \quad (48)$$

Inserting equation (48) into equation (21), considering a planar, rotationally symmetric state of stress/strain (cf. equation (3)), results in the following form for the strain tensor:

$$\boldsymbol{\varepsilon}^S = \begin{pmatrix} (\Phi_{11} + \Phi_{12})\varepsilon_{\parallel} + \Phi_{11}\varepsilon_{\perp} & (\Phi_{16} + \Phi_{26})\varepsilon_{\parallel} + \Phi_{36}\varepsilon_{\perp} & (\Phi_{51} + \Phi_{52})\varepsilon_{\parallel} + \Phi_{53}\varepsilon_{\perp} \\ (\Phi_{16} + \Phi_{26})\varepsilon_{\parallel} + \Phi_{36}\varepsilon_{\perp} & (\Phi_{12} + \Phi_{22})\varepsilon_{\parallel} + \Phi_{23}\varepsilon_{\perp} & (\Phi_{41} + \Phi_{42})\varepsilon_{\parallel} + \Phi_{43}\varepsilon_{\perp} \\ (\Phi_{51} + \Phi_{52})\varepsilon_{\parallel} + \Phi_{53}\varepsilon_{\perp} & (\Phi_{41} + \Phi_{42})\varepsilon_{\parallel} + \Phi_{43}\varepsilon_{\perp} & \varepsilon_{\perp} \end{pmatrix}. \quad (49)$$

Now compare equation (19) with equation (49). In both descriptions of  $\boldsymbol{\varepsilon}^S$  the same result holds for the strain tensor component  $\varepsilon_{33}^S = \varepsilon_{\perp}$ . However, the components  $\varepsilon_{11}^S = \varepsilon_{31}^S = \varepsilon_{23}^S = \varepsilon_{32}^S$  are equal to zero according to the constraints of the iVW model, whereas these components are generally non-zero according to equation (49). As only off-diagonal components of the tensor  $\Phi$  contribute to these components, these terms will generally be small compared with the component  $\varepsilon_{33}^S$  (note that  $\langle \Phi \rangle = \mathbf{I}$ ).

As a result, it can be concluded that the EK model in the limit of needle-shaped crystallites leads to constraints for the strain tensor components which approach, but are not equal to, those adopted in the iVW model. These findings explain, why a better agreement of the VW model with the EK model is observed for  $\eta \rightarrow 0$  than for the iVW model with the EK model for  $\eta \rightarrow \infty$ . This has been

made clear at various places in sections 3.1–3.4 presenting the results of the numerical calculations.

#### 4. Discussion

The VW and the iVW models can be used to account for the effect of surface anisotropy (anisotropic grain interaction invoked by the presence of a surface) in a polycrystal. The EK model can account for the occurrence of a morphological texture, which effectively involves overall anisotropic grain interaction. At first glance, the occurrence of surface anisotropy and the occurrence of a grain-shape texture bear no relation. However, for the special ideal grain-shape texture considered here (all ellipsoidal crystals are oriented with their principal  $a$ , axis perpendicular to the surface), the similarities in the result of the VW and the iVW models, on the one hand, and the EK model, on the other hand, can be made plausible as follows.

First, consider the limit of flat-disc shaped grains (i.e.,  $\eta \rightarrow 0$ ). In this case, the polycrystal can be conceived as a stack of flat disc-shaped grains with the discs oriented parallel to the surface (see figure 6a). If such a polycrystal is subjected to a plane, rotationally symmetric mechanical strain parallel to the disc interfaces, all discs (grains) will obviously experience the same in-plane strain. The stress acting perpendicular to the interfaces is zero at the top and bottom surfaces, as the surfaces are unloaded. Recognising the symmetry of the stack (all interfaces are equivalent) and the mechanical equilibrium conditions (force balance across the interfaces), all discs must experience the same stress (= nil, as the surface is unloaded) perpendicular to the interfaces. The grain-interaction constraints are thus of the Vook–Witt type.

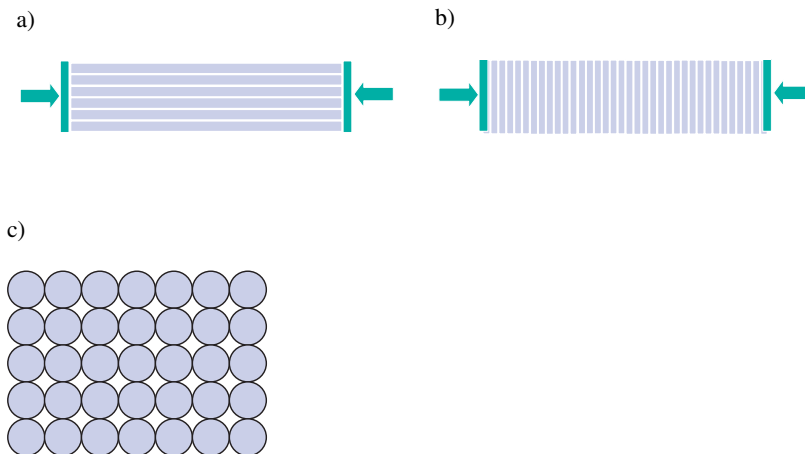


Figure 6. Sketches of polycrystals consisting of (a) flat-disc shaped grains (b) needle-shaped grains, subjected to a rotationally symmetric mechanical strain, such that contour coherency is preserved. (c) Top view on the assembly of needle-shaped grains.

Next, consider the limit of needle-shaped grains (i.e.,  $\eta \rightarrow \infty$ ). In this case, the polycrystal can be conceived as an assembly of needle-shaped grains with their needle axis perpendicular to the surface (see figures 6b and 6c).

If such a polycrystal is subjected to a plane, rotationally symmetric mechanical strain perpendicular to the needle axes, all grains will experience the same strain along the needle axes because the outer contour of the assembly should not change. With respect to the in plane direction, the grains can neither experience the same in-plane stresses nor the same inplane strains: If the grains would all experience the same in-plane stresses, the conditions of mechanical equilibrium (force balance across the contact lines) would be met: however, the strains would then be different for crystallographically differently oriented grains and the assembly would not be strained coherently laterally (cf. figure 6c). If, on the other hand, the grains would all experience the same in-plane strains, the assembly would be strained coherently laterally, but mechanical equilibrium could not occur as the stresses of crystallographically differently oriented grains would not match. In conclusion, the ‘true’ grain-interaction constraints perpendicular to the needle axes (i.e. for in-plane directions) will lie somewhere between the bounds defined by the Reuss (constant stresses) and Voigt (constant strains) models.

The above discussion elucidates the findings obtained in section 3. The EK model in the limit of needle-shaped grains leads to grain-interaction constraints with respect to the in-plane direction which approach, but are not equal to, those adopted in the iVW model (cf. equations (43) and (49) and figure 4). The grain-interaction constraints along the needle axes, however, are equal for the iVW and EK (in the limit of needle-shaped grains) models (cf. equations (44) and (49) and figure 4). As a consequence, the similarities of the EK (for needle-shaped grains) and iVW models with respect to the diffraction and mechanical elastic constants are much less pronounced than the similarities of the EK (for flat disc-shaped grains) and VW models (cf. figures 2 and 3).

Strikingly opposite to what may be expected on the basis of the above discussion, the Vook–Witt model has first been applied successfully to thin films exhibiting a columnar grain microstructure [10]. This can be understood as follows. In the latter case the boundaries (in the sputter-deposited films) are conceived to have an ‘open structure’, i.e. it can be assumed that a reduced interaction occurs across the column boundaries. The misfit (cooling induced thermal misfit) is imposed at the base of the columns, i.e. the imposed misfit strain parallel to the layer/substrate interface is the same for all columns (cubic materials, i.e. of isotropic thermal expansion, are considered). This naturally leads to the concept of equal strains parallel to the layer/substrate interface in all columns and equal stresses perpendicular to the surface of the layer (equal to nil) for all columns. Hence, Vook–Witt type of grain interaction. In contrast with this discussion, pertaining to thin films considered by van Leeuwen *et al.* [10] and Welzel *et al.* [14, 15], the grains (either flat discs, or needle-shaped grains) considered in this paper are tightly connected with each other across the grain boundaries and this explains an inverse Vook–Witt type of grain interaction for the case of the needle-shaped (say columnar-shaped) grains.

Even though it has been shown in this work that the Vook–Witt and inverse Vook–Witt models, originally introduced for the description of surface anisotropy as especially evident in thin films, exhibit similarities with the Eshelby–Kröner model,

for cases of extreme grain-shapes textures, the similarities of the Vook–Witt and the inverse Vook–Witt models with the Eshelby–Kröner model are of mathematical nature and do not imply that the Eshelby–Kröner model can be used to account for the effect of surface anisotropy; the Eshelby–Kröner model is a model for bulk polycrystals. Rather, the Vook–Witt (for flat-disc shaped grains) and inverse Vook–Witt (for needle-shaped grains) models may be used as substitutes for the mathematically much more tedious Eshelby–Kröner model. Thereby time consuming numerical integrations, cumbersome handling of tensors and the iterative procedure required in the application of the Eshelby–Kröner model may be replaced by the much less elaborate calculations in the Vook–Witt and inverse Vook–Witt models for cases of extreme grain-shape textures.

## 5. Conclusions

- Anisotropic grain interaction is induced by the presence of a surface (surface anisotropy, most clearly observed for thin films) and the occurrence of a grain-shape, morphological texture. Recently applied models for the description of surface anisotropy and grain-shape texture are the so-called Vook–Witt (VW) and inverse Vook–Witt (iVW) models and the Eshelby–Kröner (EK) model, respectively. For the case of an ideal grain-shape texture relations/similarities between results obtained from these models occur.
- Considering mechanical elastic constant, diffraction stress factors, variances of specific stress/strain tensor components and even the detailed strain/stress distributions in orientation (Euler) space, it follows that, for the case of ellipsoidal crystallites oriented with their  $a_3$  axis perpendicular to the surface, the EK model approaches the VW model if the crystallites become flat discs ( $\eta \rightarrow 0$ ) and approaches the iVW model if the crystallites become needles ( $\eta \rightarrow \infty$ ).
- These observations can be given an analytical basis by approximations of the tensor  $\Phi$  (cf. equation (21)) for flat disc shaped and needle shaped grains. It follows that the grain interaction in the EK model in these limiting cases leads to constraints for the strain tensor components compatible with those adopted in the VW and iVW models, respectively.
- It can also be proven analytically that the similarity of the VW and EK (for  $\eta \rightarrow 0$ ) models is stronger than of the iVW and EK ( $\eta \rightarrow \infty$ ) models, in full agreement with the numerical calculations.
- Hence, even though the Vook–Witt and inverse Vook–Witt models have been developed in particular to express the effect of elastic surface anisotropy of bulk polycrystals and thin films, they are capable of modelling the effect of special, limiting morphological textures on the elastic grain-interaction. Thus, time consuming numerical calculations as required in the application of the Eshelby–Kröner model can be replaced by much less elaborate calculations according to the Vook–Witt (for flat-disc shaped grain morphology) and inverse Vook–Witt (for needle-shaped grain morphology) models. This can greatly simplify numerical algorithms for the calculations of elastic and, possibly, plastic grain interaction.

## Appendix

### Analytical approximations of the $\Phi$ tensor

Consider the ideal grain-shape texture composed of ellipsoidal grains with their principal axes aligned along common directions in the specimen frame of reference. This is the homogenous matrix, instead of a matrix of spherical grains, in the current elaboration of the Eshelby–Kröner model. Following the conventions introduced in section 2, the axes of rotational symmetry of the ellipsoids coincide with the  $S_3$  axis. Hence, the polycrystal exhibits transverse elastic isotropy and thus the stiffness tensor of the specimen takes the following form in Voigt notation (see, for example, Hauk [1]):

$$\mathbf{C} = \begin{bmatrix} C_{11} & C_{12} & C_{13} & 0 & 0 & 0 \\ C_{12} & C_{11} & C_{13} & 0 & 0 & 0 \\ C_{13} & C_{13} & C_{33} & 0 & 0 & 0 \\ 0 & 0 & 0 & C_{44} & 0 & 0 \\ 0 & 0 & 0 & 0 & C_{44} & 0 \\ 0 & 0 & 0 & 0 & 0 & C_{66} \end{bmatrix}. \quad (50)$$

By inserting equation (50) into equation (24), simplifications for the tensors  $\mathbf{D}^{-1}$  can be obtained. By subsequently inserting the simplified tensor  $\mathbf{D}^{-1}$  in equation (23) and considering the limits  $\eta \rightarrow 0$  and  $\eta \rightarrow \infty$ , simplified forms of the tensor  $\mathbf{E}$  can be obtained. These calculations are cumbersome and have been conducted here employing the programme ‘Mathematica’ (Version 4.1). The following results have been obtained.

**Flat discs ( $\eta \rightarrow 0$ ):  $a_1 = a_2, a_3 \rightarrow 0$ .** For the tensor  $\mathbf{D}^{-1}$  it holds that:

$$\lim_{a_3 \rightarrow 0} \mathbf{D}^{-1} = \begin{pmatrix} H_{11} & H_{12} & H_{13} \\ H_{12} & H_{11} & H_{23} \\ H_{13} & H_{23} & H_{33} \end{pmatrix} + O(a_3^4) \quad (51)$$

where

$$H_{11} = \frac{a_3^2}{C_{44}k_3^2} \quad (52)$$

$$H_{12} = \frac{a_3^4 k_1 k_2 (C_{13}^2 - C_{12} C_{33} + 2 C_{13} C_{44} + C_{44}^2 - C_{33} C_{66})}{a_1^2 C_{33}^2 C_{44}^2 C_3^4} \quad (53)$$

$$H_{12} = -\frac{a_3^3 k_1 (C_{13} + C_{44})}{a_1 C_{33} C_{44} k_3^3} \quad (54)$$

$$H_{23} = -\frac{a_3^3 k_1 (C_{13} + C_{44})}{a_1 C_{33} C_{44} k_2^3} \quad (55)$$

$$H_{33} = \frac{a_3^2}{C_{33} k_3^2} \quad (56)$$

Insertion of equation (51) into equation (23) leads to the following simplification for the tensor  $\mathbf{E}$ :

$$\lim_{a_3 \rightarrow 0} \mathbf{E} = \begin{pmatrix} 0 & 0 & 0 & 0 & 0 & 0 \\ 0 & 0 & 0 & 0 & 0 & 0 \\ 0 & 0 & \frac{1}{C_{33}} & 0 & 0 & 0 \\ 0 & 0 & 0 & \frac{1}{4C_{44}} & 0 & 0 \\ 0 & 0 & 0 & 0 & \frac{1}{4C_{44}} & 0 \\ 0 & 0 & 0 & 0 & 0 & 0 \end{pmatrix}. \quad (57)$$

Upon insertion of equation (57) into equation (21), equation (46) is obtained.

**Needles ( $\eta \rightarrow \infty$ ):**  $a_1 = a_2, a_3 \rightarrow \infty$ . For the tensor  $\mathbf{D}^{-1}$  it holds that:

$$\lim_{a_3 \rightarrow \infty} \mathbf{D}^{-1} = \begin{pmatrix} H_{11} & H_{12} & H_{13} \\ H_{12} & H_{11} & H_{23} \\ H_{13} & H_{23} & H_{33} \end{pmatrix} \quad (58)$$

where:

$$H_{11} = \frac{a_1^2 (C_{11} k_1^2 - C_{12} k_1^2 + 2C_{11} k_2^2)}{(C_{11}^2 - C_{11} C_{12}) (k_1^2 + k_2^2)^2} \quad (59)$$

$$H_{12} = -\frac{a_1^2 (C_{11} + C_{12})}{(C_{11}^2 - C_{11} C_{12}) (k_1^2 + k_2^2)^2} k_1 k_2 \quad (60)$$

$$H_{13} = 0 \quad (61)$$

$$H_{23} = 0 \quad (62)$$

$$H_{33} = \frac{a_1^2}{C_{44} (k_1^2 + k_2^2)^2} \quad (63)$$

Insertion of equation (51) into equation (23) leads to the following simplification for the tensor  $\mathbf{E}$ :

$$\lim_{a_3 \rightarrow \infty} \mathbf{E} = \begin{pmatrix} \frac{5C_{11} - 3C_{12}}{8C_{11}^2 - 8C_{11}C_{12}} & \frac{C_{11} - C_{12}}{8C_{11}^2 - 8C_{11}C_{12}} & 0 & 0 & 0 & 0 \\ \frac{C_{11} + C_{12}}{8C_{11}^2 - 8C_{11}C_{12}} & \frac{5C_{11} - 3C_{12}}{8C_{11}^2 - 8C_{11}C_{12}} & 0 & 0 & 0 & 0 \\ 0 & 0 & 0 & 0 & 0 & 0 \\ 0 & 0 & 0 & \frac{1}{8C_{44}} & 0 & 0 \\ 0 & 0 & 0 & 0 & \frac{1}{8C_{44}} & 0 \\ 0 & 0 & 0 & 0 & 0 & \frac{3C_{11} - C_{12}}{8C_{11}^2 - 8C_{11}C_{12}} \end{pmatrix}. \quad (64)$$

Upon insertion of equation (64) into equation (21), equation (48) is obtained.

## References

- [1] V. Hauk (Editor), *Structural and Residual Stress Analysis by Non-destructive Methods* (Elsevier, Amsterdam, 1997).
- [2] U. Welzel and E.J. Mittemeijer, *J. Appl. Phys.* **93** 9001 (2003).
- [3] A. Reuss and Z. Angew. Math. Mech. **9** 49 (1929).
- [4] W. Voigt, *Lehrbuch der Kristallphysik* (Teubner, Leipzig-Berlin, 1910).
- [5] H. Neerfeld, *Mitt. K.-With.-Inst. Eisenforschg.* **24** 61 (1942).
- [6] R. Hill, *Proc. Phys. Soc.* **65** 349 (1952).
- [7] J.D. Eshelby, *Proc. Soc. A* **241** 376 (1957).
- [8] E. Kröner, *Z. Physik* **151** 504 (1958).
- [9] G. Kneer, *Phys. Stat. Sol.* **9** 825 (1965).
- [10] M. van Leeuwen, J.-D. Kamminga and E.J. Mittemeijer, *J. Appl. Phys.* **86** 1904 (1999).
- [11] J. Stickforth, *Tech. Mitt. Krupp – Forsch.-Ber.* **24** 89 (1966).
- [12] M. Leoni, U. Welzel, P. Lamparter, E.J. Mittemeijer and J.-D. Kamminga, *Phil. Mag. A* **81** 597 (2001).
- [13] R.W. Vook and F. Witt, *J. App. Phys.* **36** 2169 (1965).
- [14] U. Welzel, M. Leoni and E.J. Mittemeijer, *Phil. Mag.* **83** 603 (2003).
- [15] U. Welzel, M. Leoni and E.J. Mittemeijer, in *Diffraction Analysis of the Microstructure of Materials*, edited by E.J. Mittemeijer and P. Scardi (Springer, Berlin, 2004).
- [16] J. Krier, H. Ruppertsberg, M. Berveiller and P. Lipinski, *Textures Microstruct.* **14–18** 1147 (1991).
- [17] B.C. Hendrix and L.G. Yu, *Acta. Mat.* **46** 127 (1998).
- [18] N. Koch, U. Welzel, H. Wern and E.J. Mittemeijer, *Phil. Mag.* **84** 3547 (2004).
- [19] C. Giacovazzo, H.L. Monaco, D. Vioterbo, F. Scordari, G. Gilli, G. Zanotti and M. Catti, *Fundamentals of Crystallography* (Oxford Science, Oxford, 1998).
- [20] R.-J. Roe and W.R. Krigbaum, *J. Chem. Phys.* **40** 2608 (1964).
- [21] S.W. Tsai and H.T. Hahn, *Introduction to Composite Materials* (Technomic Publishing Co., Lancaster, Pennsylvania, 1987).
- [22] M. Mouden and A. Molinari, *Computational Materials Science* **5** 82 (1996).
- [23] R.J. Asaro and D.M. Barnett, *J. Mech. Phys. Solids* **23** 77 (1975).

- [24] T. Mura, *Micromechanics of Defects in Solids* (Kluwer, Dodrecht, 1987), p. 137.
- [25] U. Welzel, J. Ligot, P. Lamparter, A.C. Vermeulen and E.J. Mittemeijer, *J. Appl. Cryst.* **38** 1 (2004).
- [26] M.A. Meyers and K.K. Chawla, *Mechanical Metallurgy, Principles and Applications* (Prentice-Hall, Englewood Cliffs, New Jersey), p. 57.